Open Archive Toulouse Archive Ouverte (OATAO)

OATAO is an open access repository that collects the work of Toulouse researchers and makes it freely available over the web where possible.

Any correspondence concerning this service should be sent to the repository administrator: staff-oatao@inp-toulouse.fr

Electroactive influence of ferroelectric nanofillers on polyamide 11 matrix properties

Jean-Fabien Capsal, Eric Dantras [*], Jany Dandurand, Colette Lacabanne

Laboratoire de Physique des Polymères, Institut Carnot CIRIMAT, Université Paul Sabatier, Toulouse cedex 09, France

Abstract

Barium titanate ceramic powders have been incorporated in polyamide 11 to form homogeneous dispersion of particles in the matrix. Barium titanate/polyamide 11 nanocomposites have been synthesized using a solvent casting method with ultrasonic stirring to homogeneously disperse inclusions in the matrix. Composites with volume fraction of barium titanate ϕ ranging from 0.01 to 0.4 were elaborated. Films were fabricated using a hot press method. Only the inclusions were poled in the matrix to form a ferroelectric particles/unpoled matrix composite. Interactions between the particles and the matrix, pyroelectric and piezoelectric response were studied as a function of ϕ by dynamic dielectric spectroscopy. Composites show interesting pyro-piezoelectric activity. Pyroelectric merit factor increases linearly and it reaches a limit value of 0.3 for a volume fraction $\phi = 0.1$.

1. Introduction

During last years, some ferroelectric polymers were studied as P(VDF) [1], P(DVF-TrFE)[2], PA 11 [3,4]. To increase the electroactive properties of polymers, ferroelectric fillers were introduced in these polymer matrix to form ferroelectric polymer/ferroelectric fillers composites [5,6]. Most of these works concern P(VDF-TrFE) based composites. We propose to associate ferroelectric properties of inorganic materials with the attractive mechanical properties of polymers. Barium titanate (BT) is one of the most used ferroelectric ceramic, known for its high permittivity, high piezoelectric and pyroelectric properties [7]. As the tetragonality of BT decreases with the particles mean diameter [8,9], we choose particles of about 700 nm in diameter. PA 11 has been used as matrix in its non poled state and ceramic powder was incorporated to form homogeneous dispersion of particles in the matrix (0–3 composites). Ferroelectric properties of the composites poled under 20 kV/mm (only ceramic phase poled) have been studied by changing the volume fraction of BT. The challenge is to insure a synergy between the electroactive properties of the ceramic and the attractive engineering behavior of PA 11.

2. Experimental section

2.1. Materials and sample preparation

Polyamide 11[1] (PA 11) will be studied in its unpoled state. Barium titanate nanopowders (BaTiO$_3$) are well known for their high ferroelectric properties. The mean diameter of these nanoparticules is 700 nm. PA 11 powder was dissolved in a solution of dimethyl acethyl amide (DMAc) and the required barium titanate powder was

---

[*] Corresponding author. Tel.: +33 561556456; fax: +33 561556221.
   E-mail address: dantras@cict.fr (E. Dantras).

[1] PA 11 was supplied by Arkema (France) and BaTiO$_3$ by Inframat materials (USA).

dispersed to form a mixture by ultrasonic stirring. The samples were dried over night at 110 °C to remove the solvent. The nanocomposites were hot pressed to form thin films of thickness from 70 to 100 μm. Volumic ratios (ϕ) of nanoceramic in nanocomposite films were 0.01, 0.024, 0.1, 0.2, and 0.4. For dynamic dielectric measurements, gold electrodes were evaporated on both sides of thin films by cathode pulverization. For pyroelectric and piezoelectric measurements nanocomposites were poled to orient the dipoles; a macroscopic polarization P was obtained. The films were polarised under vacuum (at room temperature under low pressure $p = 2 \times 10^{-4}$ hPa) to prevent any voltage breakdown. Electric signal was generated by a ± 10 V generator and then amplified using a $\times 2000$ voltage amplifier. The electric field E is increased progressively until 20 kV/mm and kept constant 30 min. It was removed before short-circuited. During poling, the current versus the applied field was measured [10]. The samples were short-circuited to relax the internal stress induced during the poling and then annealed at 100 °C to eliminate thermally stimulated current during the pyroelectric measurements.

2.2. Scanning electron microscopy

JEOL JSM 6700F – Scanning electron microscope with field emission gun (SEM-FEG) was used to study BT dispersion in the polyamide matrix. As BT density is higher than the polyamide density, backscattered electron detection was used. Energy dispersive X-ray spectroscopy was made on the samples in order to verify the BT trace in the matrix.

2.3. Standard differential scanning calorimetry

Standard differential scanning calorimetry (DSC) measurements were performed using a DSC/TMDSC 2920 set up. The sample temperature was calibrated using the onset of melting of tin ($T_m = 231.88$ °C), indium ($T_m = 156.6$ °C) and cyclohexane ($T_m = 6$ °C) with a heating rate of $q_h = +5$ °C min^{-1}. The heat-flow was calibrated with the heat fusion of indium ($\Delta H = 28.45$ J g^{-1}), its baseline was corrected with sapphire. DSC experiments were systematically carried out over a temperature range from the equilibrium state (in order to remove the effect of previous thermal history) $T_{eq} = T_m + 20$ °C down to the glassy state $T_0 = T_g - 70$ °C with a constant cooling rate $q_c = +20$ °C min^{-1}, and followed by a linear heating rate $q_h = -10$ °C min^{-1}. For each sample, the glass transition temperature (inflection point method) range but also the specific heat jump was measured by a standard DSC during a heating scan ($q_h = +10$ °C min^{-1}).

2.4. Isothermal dielectric spectroscopy

Dynamic dielectric spectroscopy (DDS) were performed using a BDS400 covering a frequency range of 10^{-2} Hz–3×10^6 Hz with 10 points per decade. Experiments were carried out in a temperature range from -150 °C to 150 °C. Dielectric isothermal spectra were measured every 5 °C. Before each frequency scan, temperature was kept constant to ± 0.2 °C. The real ε'_T and imaginary ε''_T parts of the relative complex permittivity ε^*_T were measured as a function of frequency f at a given temperature T. Experimental data are fitted by the Havriliak–Negami (HN) function with an additional conductivity term [11]

$$\varepsilon^*_T = \varepsilon_\infty + \frac{\varepsilon_{st} - \varepsilon_\infty}{[1 + (i\omega\tau_{HN})^{\alpha_{HN}}]^{\beta_{HN}}} - \frac{i\sigma_0}{(\varepsilon_{st}\omega)}, \quad (1)$$

where ε_∞ is the relative real permittivity at infinite frequency, ε_{st} is the relative real permittivity at null frequency, τ_{HN} is the relaxation time, ω is the angular frequency, α_{HN} and β_{HN} are the Havriliak–Negami parameters.

2.5. Pyroelectric and piezoelectric measurements

Pyroelectric measurements were performed by a femtoamperemeter. The samples were short-circuited during 5 min at room temperature and cooled to -170 °C. They were heated up to 100 °C with a constant heating rate ($q_h = +7$ °C min^{-1}) to eliminate thermally stimulated currents. Then, they were cooled again to -170 °C and the pyrocurrent was recorded as a function of temperature. The pyroelectric coefficient p is proportional to the heating rate and to the sample surface as [12]

$$p = \frac{i(T)}{\beta * S}, \quad (2)$$

where $i(T)$ is the current (A) as a function of temperature, S is the surface (m^2), β (or q_h) is the heating rate (°C min^{-1}). Piezoelectric measurements were carried out using a PM 200 piezometer supplied by Piezotest,UK, with a strength of 0.25 N at 110 Hz in frequency. These measurements were carried out after the pyroelectric tests to prevent any poling effect (internal stresses).

3. Results and discussion

3.1. Dispersion

The dispersion of barium titanate nanopowder in the polymeric matrix has been studied by scanning electron microscopy (SEM) in order to check the experimental protocol. Fig. 1(a) shows a good dispersion of BT in the matrix for a low volume fraction ($\phi = 0.024$) at a microscopic scale. The magnification of one part of Fig. 1(a) is represented in Fig. 1(b). Spherical particles of BT (nanometric scale) are homogeneous dispersed in PA11. The chemical nature of inclusion has been studied by energy dispersive X-ray spectroscopy. The EDX spectrum is reported in Fig. 1. As expected, the characteristic peaks of BaTiO$_3$ are pointed out. A platinum trace caused by pollution is marked. An equivalent study has been performed on an amorphous area: peak characteristic of C and N atoms (major chemical constituents of PA 11) are present. Nano-
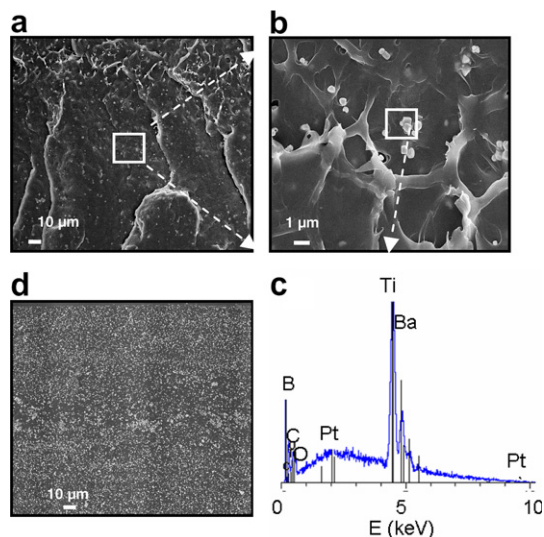
Fig. 1. FEG-SEM pictures of PA11 + BaTiO$_3$ nanocomposites for (a) ϕ = 0.024 (×1000), (b) ϕ = 0.024 (×5000), (c) EDXS of inclusions and (d) ϕ = 0.1

Fig. 2. PA 11 melting peak in 0–3 nanocomposites obtained by DSC.

Fig. 3. DSC thermograms of PA11, BaTiO$_3$ 700 nm nanoparticles and nanocomposites with volume fraction ϕ ranging from 0.01 to 0.4.

composites with higher volume ratio (ϕ = 0.1) of BaTiO$_3$ were also elaborated. SEM experiments were carried out and the micrographs confirm that even at high volume fraction of nanoparticles in the matrix the dispersion is still correct at a nanometric scale. These results were confirmed by thermogravimetry analysis. The values of inorganic residue remain constant for several samples. These measurements have shown an accuracy of the dispersion of less than 3% in weight even for high volume ratio (ϕ = 0.4). Samples are homogeneous at a macroscopic scale.

3.2. Thermal transitions

3.2.1. Polyamide 11 melting

Differential scanning calorimetry measurements were performed on the nanocomposites in order to estimate the influence of BaTiO$_3$ volume fraction on the PA 11 crystallinity ratio. The thermograms showing the PA 11 melting peaks are reported in Fig. 2. The crystallinity ratio, χ_c, deduced from the melting enthalpy (ΔH_m) is estimated at 27%. Nanoparticles, even at high volume ratio, do not modify the crystallinity of the matrix. But, we note that the melting peak of nanocomposites is shifted to lower temperatures as the volume ratio increases. It has been attributed to structural defects within crystallites.

3.2.2. BaTiO$_3$ Curie point

DSC thermograms of PA 11, BaTiO$_3$ and nanocomposites, in the temperature range (100–160 °C) are shown in Fig. 3. We observe that the nanoparticles of barium titanate exhibit an endothermic peak at 130 °C characteristic of a first order transition. Polyamide does not have any transition in this temperature range. This event has been attributed to the ferro/paraelectric transition, also called Curie point.
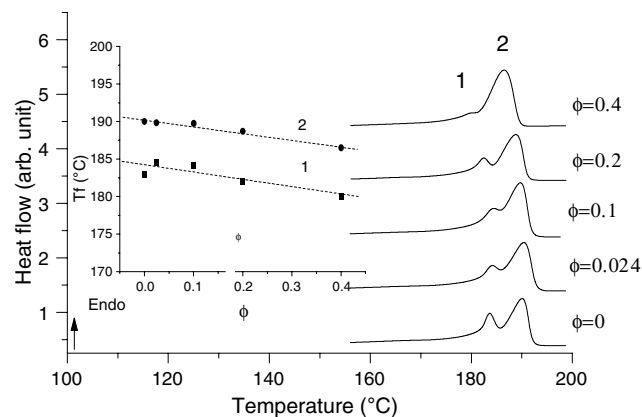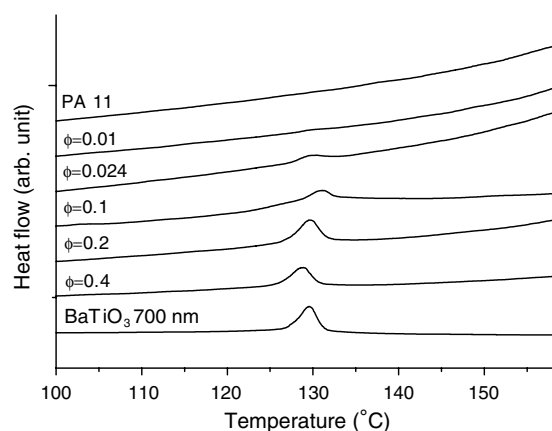
The amplitude of the ferroelectric to paraelectric transition increases with the volume ratio of barium titanate. Thermal manifestation associated with the Curie point appears with ϕ = 0.024 volume fraction of barium titanate. This fact shows that ferroelectrics properties can be observed even at low volume fraction.

3.3. Dielectric properties

Broadband dielectric spectroscopy was performed to estimate the influence of nanofillers on the molecular mobility of the polyamide amorphous phase. The Havriliak–Negami equation permits us to extract the relaxation times associated with the various modes. The evolution of the relaxation time of the γ and α modes has been reported on an Arrhenius diagram (Fig. 4). The γ mode is associated with the local mobility of the aliphatic sequences and the α mode is attributed to the dielectric manifestation of the glass transition of the polyamide 11 [13]. β mode is not reported due to its high sensitivity with thermal history and water content. Fig. 4 shows the evolution of relaxation times as a function of BaTiO$_3$ ratio. It confirms that molecular mobility is independent of the nanoceramics ratio. As there are very few interactions
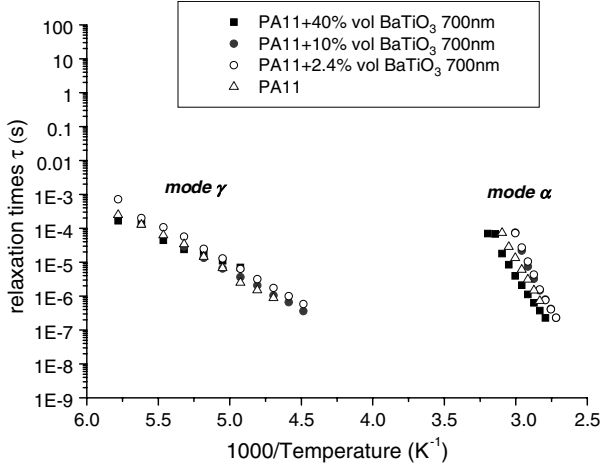
Fig. 4. Relaxation times versus temperature of polyamide 11 and nanocomposites with volume fraction $\phi = 0.024$, $\phi = 0.1$ and $\phi = 0.4$.
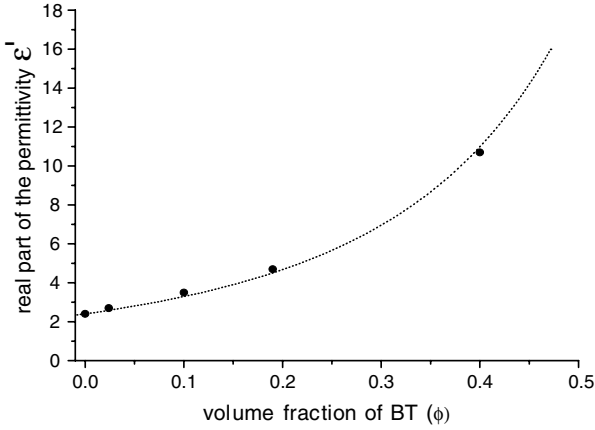

Fig. 5. Increase of relative permittivity of nanocomposites with the volume fraction of BaTiO$_3$. Dot line is the fit of Bruggeman model.

between nanoparticules and matrix, the molecular mobility of PA 11 is not disturbed.

One of the routes to greatly increase the dielectric permittivity is to incorporate particles with high dielectric permittivity. The evolution of dielectric permittivity with volume ratio of BaTiO$_3$ is predicted by the Bruggeman model [14].

Fig. 5 shows that the evolution of ε' at room temperature as a function of volume fraction is well fitted with the Bruggeman model. From this model we can estimate the relative permittivity of the barium titanate nanopowder. It has been found that ε' is equal to 1500 at room temperature. Recent experiments of SPS (Spark plasma sintering) on nanopowders [15] allows us to measure the value of ε' in the bulk state. The dielectric permittivity ε' has been estimated at 2000 (room temperature). These data are coherent with the Bruggeman model.

3.4. Electroactive properties

In order to determine the ferroelectric properties, the samples were polarised as described in experimental sec-

tion. As the polarization field of stretched PA 11 is 100 kV/mm, only BaTiO$_3$ nanofillers in the nanocomposites are poled. Fig. 6 reports the values of piezoelectric coefficient at room temperature. The piezoelectric coefficient d increases linearly with the volume fraction until the value of 1 pC/N ($\phi = 0.2$). We recall that d is equal to 5 pC/N for ferroelectric polyamide 11 [16]. This value is of the same order of magnitude than the one obtained for nanocomposites with non poled PA 11 with poled nanoparticles. Pyroelectric activity has been reported in Fig. 6. We observe a quasi linear increase of p_3 with the volume fraction of BaTiO$_3$. This behavior is described using the linear mixture rule of the pyroelectric (p) and piezoelectric coefficient (d) [17]

$$p = \alpha_c L_E p_C \cdot \phi + \alpha_p p_P \cdot (1 - \phi), \tag{3}$$

$$d = \alpha_c L_E d_C \cdot \phi + \alpha_p d_P \cdot (1 - \phi), \tag{4}$$

where the subscripts C and P denote the ceramic and polymer respectively, $L_E = \frac{3\varepsilon}{(2+\phi)\varepsilon+(1-\phi)\varepsilon_c}$ is the local field coefficient and α the poling ratio.

Since polyamide is in its non poled state, $p_P = 0$ μC/K/m^2 and $d_P = 0$ pC/N. In a first approximation, we find with
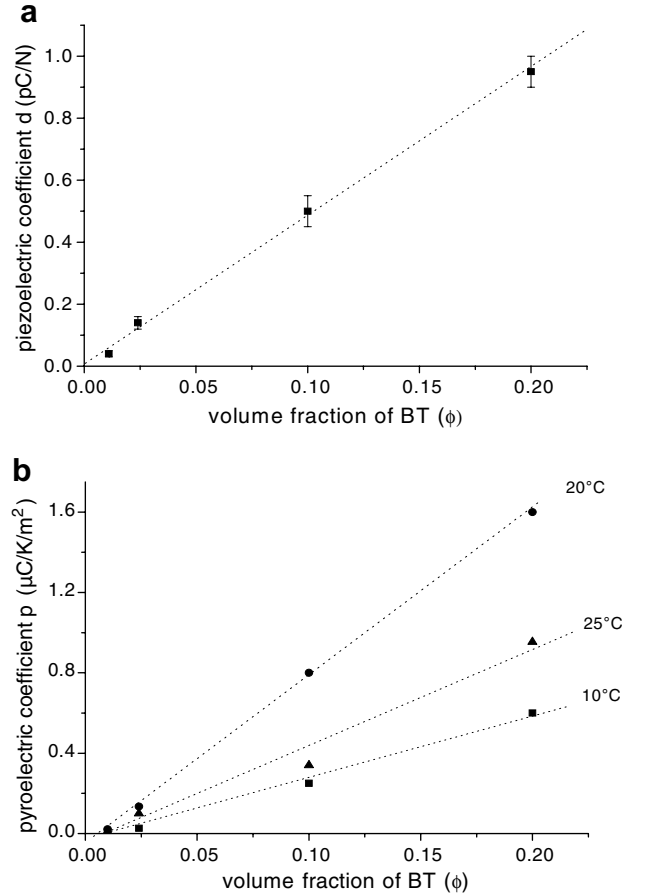

Fig. 6. Ferroelectric properties versus volume fraction of PA11/BaTiO$_3$ nanocomposites (a) piezoelectric coefficient and (b) pyroelectric coefficient (lines are drawn as guides for the eyes).

a good agreement a linear increase of the pyroelectric coefficient and piezoelectric coefficient with ϕ as previously shown in our experimental data. According to the model, it means that $\alpha_c = 1$, particles are supposed to be fully poled. In this work, particles are poled at saturation in regards of their crystallographic orientations with respect to the applied field.

We note that the pyroelectric coefficient is not constant with the temperature. A maximum value of $p = 1.5 \, \mu C/K/m^2$ is obtained at 20 °C and decreases to $p = 0.9 \, \mu C/K/m^2$ at 25 °C. It has been attributed to the orthorhombic to tetragonal phase transition of the barium titanate nanoparticles [5]. It has been confirmed by DDS measurements of $BaTiO_3$ powders as shown in Fig. 7. DDS measurements pointed out three dielectric manifestations of solid–solid transitions: respectively the rhombohedral to orthorhombic phase transition, the orthorhombic to tetragonal phase transition and the tetragonal to cubic (Curie point) around 130 °C. Eqs. (3) and (4) permit us to fit p/L_E and d/L_E versus ϕ. These equations confirm the linear increase of piezoelectric and pyroelectric coefficient with BT volume fraction.

By fixing the pyroelectric coefficient of BT at $200 \, \mu C/K/m^2$ we observe in Fig. 8 that the increase of p of the composites is higher than the predicted one.

Fig. 9 shows the evolution of the merit factor ($F_p = p/\varepsilon'$) of the nanocomposite as a function of volume ratio of $BaTiO_3$. F_p increases to a value 0.3 for $\phi = 0.1$. As the voltage response of a pyroelectric sensor is proportional to the merit factor, we conclude that nanocomposites with $\phi = 0.1$ exhibit the best properties as regards to its mechanical properties.
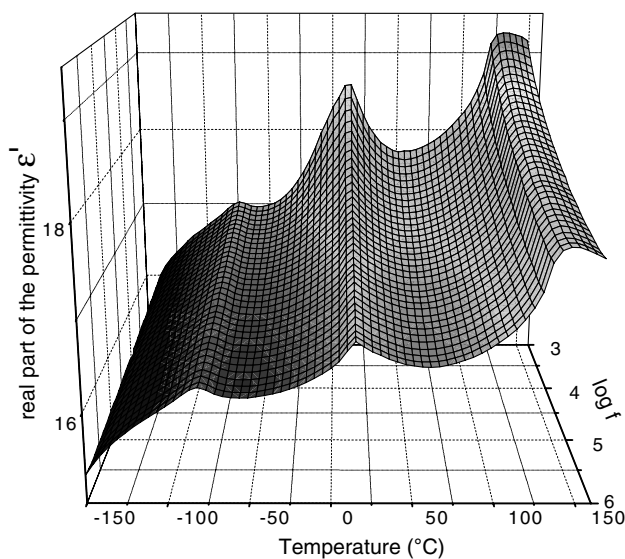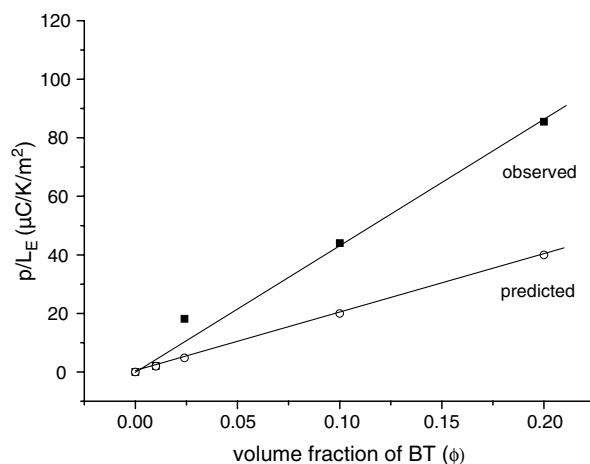

Fig. 8. Pyroelectric coefficient normalized by the local field coefficient of each sample versus ϕ at 25 °C. Solid line is the fit of Eq. (2).
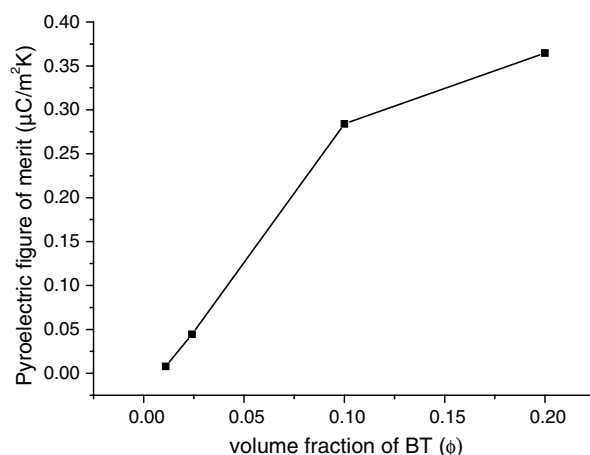

Fig. 9. Merit factor p/ε of the 0–3 nanocomposites versus volume fraction (line is drawn as guide for the eyes).

4. Conclusion

$BaTiO_3$/PA11 nanocomposites with $BaTiO_3$ volume fraction ranging from 0.01 to 0.4 have been elaborated and characterized. As the nanocomposites were poled at 20 kV/mm, only ceramic part was poled. Piezoelectric and pyroelectric activities of the composite were studied by varying nanofillers volume fraction. Suitable ferroelectric properties of the composites were obtained close to the ferroelectric properties of poled PA11. Pyroelectric merit factor increases linearly and it reaches a limit value of 0.3 for a volume fraction ϕ equal to 0.1.

Fig. 7. Real part of the permittivity of $BaTiO_3$ 700 nm nanopowders as a function of temperature and frequency.

References

[1] L. Ibos, A. Bernes, C. Lacabanne, Ferroelectrics 320 (2005) 483.
[2] G. Teyssedre, C. Lacabanne, Thermochim. Acta 226 (1993) 65.
[3] S. Ikeda, T. Saito, M. Nonomura, T. Koda, Ferroelectrics 171 (1995) 329.
[4] L. Ibos, C. Maraval, A. Bernès, G. Teyssèdre, C. Lacabanne, S.-L. Wu, J.I. Scheinbeim, J. Polym. Sci. B 37 (1999) 715.
[5] T. Furukawa, K. Ishida, E. Fukada, J. Appl. Phys. 50 (1979) 4904.

[6] K.H. Lam, H.L.W. Chan, Comp. Sci. Technol. 65 (2005) 1107.

[7] T.A. Perls, T.J. Diesel, W.I. Dobrov, J. Appl. Phys. 29 (1958) 1297.

[8] S. Wada et al., Ceram. Eng. Sci. Proceed. 26 (2005) 89.

[9] T. Yan, Z.-G. Shen, W.-W. Zhang, J.-F. Chen, J. Mater. Chem. Phys. 09 (2005) 450.

[10] F. Bauer Nuclear Instruments and Methods in Physics Research Section B: Beam Interactions with Materials and Atoms, 105 (1995), 212.

[11] S. Havriliak, S. Negami, J. Polym. Sci. Polym. Symp. 14 (1966) 99.

[12] L. Ibos et al., J. Polym. Sci. Part B 37 (1999) 715.

[13] L. Ibos, A. Bernes, G. Teyssedre, C. Lacabanne, S.-L. Wu, J.-I. Scheinbeim, Electrets (1999) 623.

[14] D.A.G. Bruggeman, Ann Phys Leipzig 24 (1935) 635.

[15] S. Guillemet-Fritsch, M. Boulos, B. Durand, V. Bley, T. Lebey, J. Eur. Ceram. Soc. 25 (2005) 2749.

[16] S. C Mathur, J.I. Scheinbeim, B.A. Newman, J. Appl. Phys. 56 (1984) 2419.

[17] T. Furukawa, K. Fujino, E. Fukada, Jpn. J. Appl. Phys. 15 (1976) 2119.